Engineered interphase mechanics of nacre-like composite structures

P.R. Budarapu[a,*], S. Thakur[a], S. Kumar[b], M. Paggi[c]

[a] *School of Mechanical Sciences, Indian Institute of Technology, Bhubaneswar 752050, India.*
[b] *Masdar Institute of Science and Technology, Khalifa University of Science and Technology, Abu Dhabi, UAE*
[c] *IMT School for Advanced Studies Lucca, Piazza San Francesco 19, 55100 Lucca, Italy*

Abstract

Nacre, also known as the mother of pearl is found in the internal layer of some seashells of gastropods and bivalves has a structure mainly made up of hard and brittle ceramic bricks of Aragonite (CaCO3) surrounded by the organic/polymer matrix which bonds ceramic bricks together in the form of brick-mortar structure. Although the percentage composition of polymer is ≈5% by weight, the presence of polymer as an interlayer between the bricks significantly enhances the toughness characteristics of the brittle Aragonite. In this study, an attempt is made to study the mechanics of nacre-like brick-mortar structure through numerical simulations. The shear stress distribution in the matrix of nacreous composites is found to be non-homogeneous due to the load transfer mechanism in brick-mortar structure, this non-homogeneity is successfully reduced by grading the modulus of matrix material which could considerably enhance the performance of the nacreous composite. The different parameters which influence the non-homogeneous stress distribution are also studied which showed these parameters can be effectively controlled to reduce the non-homogeneity in the stress distribution and reduce the peak stresses. These studies could serve as a guideline in designing nacreous composites. To use the nacreous composite as a bulk structural material, material combinations for bricks and polymer are suggested which showed promising results as their load transfer structure is similar to the nacre.

Keywords: BTMS.

1. Introduction

Nacre is found in the inner layer of mollusc shells [1, 2], enclosing the mollusc's internal organs [2] to protect the soft and delicate visceral mass [3, 4, 5]. The inner layer of mollusc is surrounded by a tough and strong outer shell grown by the mantle. The shell structures are largely made up of either Calcite or Aragonite, with a small amount of organic material primarily composed of proteins and polysaccharides. The outer calcite layer is hard against penetration, however, susceptible to cracking due to its brittle nature. On the other hand, the inner nacre layer is ductile in nature and can sustain large deformations. Nacre structure is made up of 95% of brittle aragonite (calcium carbonate) and the rest organic material [6]. The fracture toughness of the nacre structure is observed to be more than 3000 times that of pure $CaCO_3$ [7, 8], whereas, its strength is reported to be few 1000 times higher than aragonite [6]. These extraordinary mechanical properties of nacre structure are achieved through the arrangement of hard Aragonite bricks in a soft polymer matrix, resulting in a brick-mortar arrangement. The lack of strength and toughness characteristics of $CaCO_3$ are overcome by the soft polymer interlayers between the brittle bricks. As a result, tablet sliding due to the weak polymer interface layer is found to be the dominating deformation mechanism in nacre [9, 10]. Hence, the structure undergoes large deformations before propagation of possible cracks in the shell.

Presence of moisture in nacre has a vital effect on its mechanical response. Wet nacre exhibits a behaviour similar to a ductile material in tension [6]. Whereas, dry nacre shows brittle response similar to bulk aragonite [11]. This is because, without moister the organic part of nacre loses its strength and ductility. Similar behaviour is observed in the shear test of dry and wet nacre, where the shear strength of wet nacre is observed to be more by 50 MPa than that of dry nacre [11]. The reported values of stiffness, strength and toughness of nacre are: 60 GPa, 140 MPa and 1.24 kJ/m^2 [12, 13], resepctively. On the other hand, the strength and stiffness of aragonite plates is estimated to be 300 MPa and 100 GPa, respectively [10].

The structure of nacre in molluscs is naturally optimised (over millions of years) for tensile strength in the direction of the tablet length and resistance to cracks running across the tablets [14]. Large deformations in nacre are generated through various mechanisms, particularly tablet sliding [15]. Tensile stresses are channelled from tablet to tablet through shear transfer in the overlap regions and the tablets start to slide on each

*Corresponding author. Tel: +91-674-712-7134
Email address: pattabhi@iitbbs.ac (P.R. Budarapu)

other, generating voids in the process. Therefore, the deformation of nacre is dominated by tablet sliding until the potential sliding sites are exhausted [6]. As a result, tensile loading along the tablet length direction increases the strain, finally leading to the material hardening and hence spreading the inelastic deformations throughout the specimen. This is followed by specimen failure through pull-out of the tablets from the polymer matrix. Hence, in order to allow large deformations in nacre, strong and small sized tablets with a weak interphase are the desirable properties.

The extraordinary toughness and strength characteristics of nacre structure have been explained through several toughening features and mechanisms, like: micro-structural design [10], small size scale of the building blocks [13, 16], abrupt steps on the tablets surfaces [17], nano-asperities on the tablets surface [18, 19, 12], mineral bridges across the interfaces [17], visco-plastic deformation of the organic material [20, 21] and nano-structured tablets [22]. Although the above mentioned models explain various reasons for the extraordinary toughness and strength characteristics of nacre, a mechanism that can explain its properties in totality is not yet available [23]. In this context, considering the extraordinary properties of nacre structure, engineering artificial nacreous structures will be beneficial in many practical applications. However, the strength and toughness of artificial nacreous composites reported till date are observed to be much lower than the theoretically predicted values [24]. Inspite of several analytical and computational models, such as: shear lag model [10], micro-mechanical model [25], fracture-based model [16] and finite element models [18, 26, 19], to name a few, exists in the literature, the design guidelines to produce high-performance nacreous composites are yet to be reported.

An attempt is made here to study the mechanics of nacre-like brick and mortar structures through numerical simulations. The influence of various parameters like the overlap length of tablets and, thickness and modulus of the polymer layer on the performance characteristics of brick-mortar structure are investigated. The Young's modulus of the polymer layer is graded to smooth out the stress concentration regions, such that the onset of tablet separation can be delayed. The elastic modulus is functionally graded based on the deformation behaviour of the nacre structure. As a result, the amplitude of peak stresses is reduced and hence the fracture toughness is increased. Therefore, the developed bio-mimicked nacre-like structure possess high strength and toughness properties, apart from the lightweight. In general, high toughness, strength, and light weight are the most desirable properties of mechanical structures. The novelties of the present study are: (i) a numerical framework to simulate the nacre-like brick-mortar structures with engineered interfaces to arrive at the desired characteristics, (ii) influence of various parameters on the mechanical and fracture properties of nacreous structure and (iii) application of the developed numerical framework to design nacre-like metal matrix composites.

The arrangement of the manuscript is as follows: design of the regularly staggered nacreous structures is introduced in Section 2, where the modelling aspects and deformation characteristics are analysed through a numerical framework as discussed in Sections 2.1 and 2.2, respectively. Based on the deformation characteristics of the regularly staggered nacreous structure, the Young's modulus of polymer layer is functionally graded to iron out the stress peaks, as explained in Section 3. Section 4 is dedicated for a parametric study to pin-point the influence of various parameters as well as their combination on the mechanical behaviour of nacreous structures. The developed numerical framework is applied to design nacre-like metal matrix composites discussed in Section 5. Section 6 concludes the manuscript with conclusions and future scope.

2. Regularly staggered nacreous structure

The structure of nacre in seashells consists of ceramic plates and biopolymer, in the form of brick-mortar structure [9]. The polygonal ceramic plates/tablets are 5-8 μm in diameter with an average thickness of 0.5 μm. These tablets are separated by a 20-30 nm thick biopolymer layer [11]. The brittle aragonite plates are generated through a complex bio-mineralization process [3]. The aragonite plates were initially believed to be flat [25], however, later studies revealed their waviness [11]. The polymer (interphase) layer is composed of several species of biopolymer organised in multiple layers [3]. Furthermore, the aragonite tablets contains nano-grains of 30 nm in size, surrounded by a fine network of the polymer matrix. Such nanoscale features are also found in the polymer layer. The polymer layer is porous in nature with pore sizes of the order of 20-100 nm. These pores provide space for direct aragonite connection between the plates, known as nano-asperities and mineral bridges [12]. Size of such nanoscale features ranges from 10 to 30 nm, with a spacing of 100-200 nm.

2.1. Modelling aspects

In this study, numerical simulations are performed on the staggered regular nacre structure, as well as the nacreous structure with engineered interphase. A schematic arrangement of brick and polymer in nacre structure is indicated in Fig. 1(a). The structure in Fig. 1(a) is arrived based on the scanning electron microscope (SEM) images [27]. A close up of the brick-mortar structure at meso-scale is shown in Fig. 1(b) and the polymer chains at nano-scale are highlighted in Fig. 1(c). The regular staggered structure refers to a nacre structure by

staking adjacent bricks in a regular fashion, with a 50% overlap of two adjacent tablets, see Fig. 1(d). Based on its repetitive nature, a representative volume element (RVE) as indicated in Fig. 1(d), is adopted in all numerical simulations performed using the commercial software ANSYS.

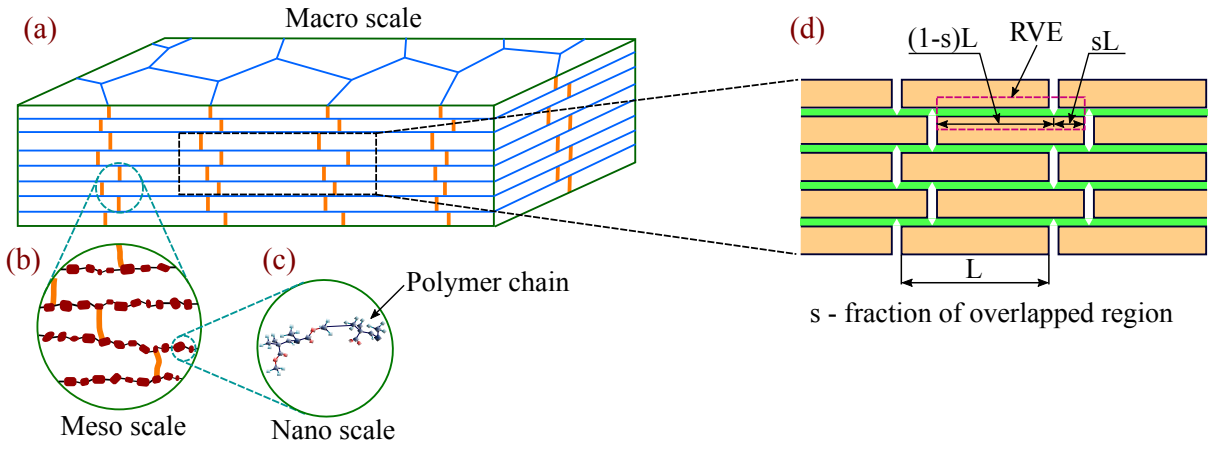

Figure 1: (a) Schematic arrangement of polygonal ceramic tablets embedded in a polymer matrix, at macro scale. A close up of the (b) brick-mortar structure at meso scale and (c) polymer chains at nano-scale. (d) A zoom of the brick-mortar structure along the thickness direction.

In this study, the adopted RVE is modelled in two dimensions in order to perform plane stress analysis. The selected RVE consists of one full tablet and two half tablets of aragonite separated by a thin interphase (polymer layer), as shown in Fig. 2. Properties of the RVE used in the numerical analysis are listed in Table 1. The dimensions of RVE elements shown in Fig. 2(a) are as follows: length of the full tablet is equal to 8 μm with a thickness of 0.4 μm, while the thickness of the polymer layer is 0.025 μm [27]. The aragonite tablet is modelled as an isotropic material with Young's modulus and Poisson's ratio equal to 100 GPa and 0.3, respectively. While the considered elastic modulus and Poisson's ratio of the interphase are 2.8 GPa and 0.4, respectively [28].

Constituent	Young's modulus (GPa)	Poisson's ratio	Length (μm)	Thickness (μm)
Aragonite (brick)	100	0.3	8	0.4
Polymer (interphase)	2.8	0.4	—	0.025

Table 1: Material properties of the regularly staggered brick-mortar structure used in the numerical analysis. The above properties are selected as the reference values for further analysis in Sections 3 and 4.

The 8-noded 'Plane183' element with each node having two degrees of freedom is adopted to discretise the RVE. After initial convergence studies, an element size of 10 nm is chosen across the entire domain. This resulted a total of 66477 elements, with 201194 nodes. Figure 2(c) shows a closeup of the discretization around the joint region of tablets, highlighting the fine discretization in the polymer. The selected boundary conditions are depicted in Fig. 2(b). All the degrees of freedom of the nodes along the left edge of the lower full tablet are arrested along the x and y directions, see Fig. 2(b). On the other hand, displacements are prescribed on the nodes along the right edge of the upper right tablet, represented by an arrow in Fig. 2(b). Furthermore, in order to ensure the symmetry boundary conditions along the y direction, displacements along the y-direction are restricted for the nodes along the upper edge of the upper tablets, as well as the lower edge of the lower tablets, denoted by roller boundary conditions in Fig. 2(b). The selected boundary conditions on RVE generates sliding motion of the tablets along the x-direction.

2.2. *Interfacial shear stress*

Displacement load is specified on the right edge of the upper right tablet (see Fig. 2(b)) such that tablet sliding is initiated. The loading is continued until the tablets are pulled out of the polymer matrix. The total specified displacement is solved in several load steps and the deformed configurations of the RVE at each step are captured. A close up of the shear stress distribution around the joint region is plotted in Fig. 2(d), where a symmetric distribution about a vertical in the joint region is evident. In this study, interfacial shear stresses represent the shear stresses in the middle of the polymer layer, extracted at element nodes along a line parallel to the x-axis, i.e. line AB shown in Fig. 3(a). Figure 3(b) shows the variation of the interfacial shear stress along the line AB. The data in Fig. 3(b) denotes the normalised interfacial shear stress as a function of the normalised length. Interfacial shear stresses are normalised by dividing them with the maximum shear stress (τ_{max}). The

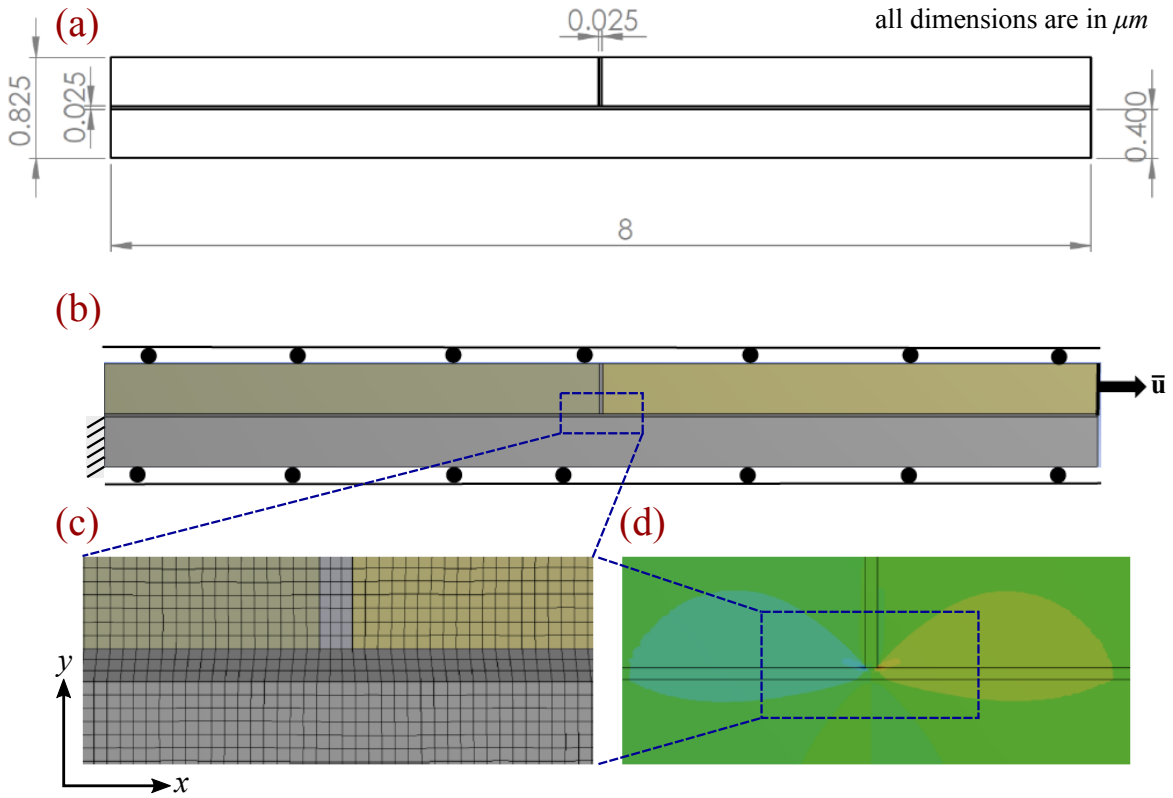

Figure 2: Modelling details of the representative volume element (RVE): (a) dimensions of the RVE expressed in micro-metres (μm), (b) specified boundary conditions superimposed on the discretized RVE, (c) a closeup of the discretization around the joint region of tablets, highlighting the fine discretization in the polymer layer and (d) the distribution of shear stress in the tablets and polymer around the joint region. The shear stress distribution in (d) is plotted in a larger area than the region in (c), in order to highlight the symmetric distribution about a vertical in the joint region.

peak shear stress estimated using the properties in Table 1 is denoted as τ_{ref}. In other words, for regularly staggered nacre structure $\tau_{max} = \tau_{ref}$. Similarly, the Young's modulus is normalised by dividing with reference modulus listed in Table 1 and distances along the tablet length are normalised with the length of the tablet. The normalised quantities are denoted by a '*' in the superscript. For instance normalised interfacial shear stress, Young's modulus, thickness and distance are indicated by $\tau*$, E*, t* and x*, respectively.

The interfacial shear stress distribution plotted in Fig. 3(b) is observed to be skew symmetric about the vertical axis at the meeting point of the upper tablets, as well as about the vertical axis at the middle of each upper tablet. Furthermore, Figure 3(b) also compares the interfacial shear stresses from the present analysis with the analytical results published in [28]. Results in Fig. 3(b) are observed to be in agreement with each other, where the maximum %error in the interfacial shear stress between the numerical and analytical results is estimated as 7%.

The load transfer in brick-mortar structures happens through shear transfer [29]. In other words, the external load will be transferred to the tablets through shear stresses in the interphase layer. The peaks of the interfacial shear stresses shown in Fig. 3(b), are observed to be concentrated at the edges of the upper tablets. As a result, the peaks are observed at the edges of the upper tablets, where a steep drop within ≈10% of the tablet length from either edge is noticed. Therefore, when the magnitude of peak stresses exceeds the permissible stresses in the polymer, the polymer layer fails by shear initiating a nano/micro-crack. Such sub-scale cracks when accumulated around a particular region, they combine to form cracks of considerable size. Upon continuous loading the accumulated sub-scale cracks continue to grow, ultimately leading to the failure of the polymer and hence the tablets will be pulled out of the polymer matrix. Therefore, design of the interphase layer in nacre structure plays a crucial role to enhance its fracture toughness.

Based on the above observations, failure of the polymer layer and hence the tablet separation could be delayed by reducing the peak interfacial shear stresses around the edges of the tablets. Reduced peak stresses will allow the polymer to absorb larger strains, thereby increasing the fracture toughness. In this study, the objective is achieved by functionally grading the elastic modulus of the interphase, following various grading laws. Furthermore, a parametric study is also conducted here to investigate the influence of different parameters like: the overlap length and, thickness and elastic modulus of the interphase, and their combination, on the interfacial shear stress distribution.

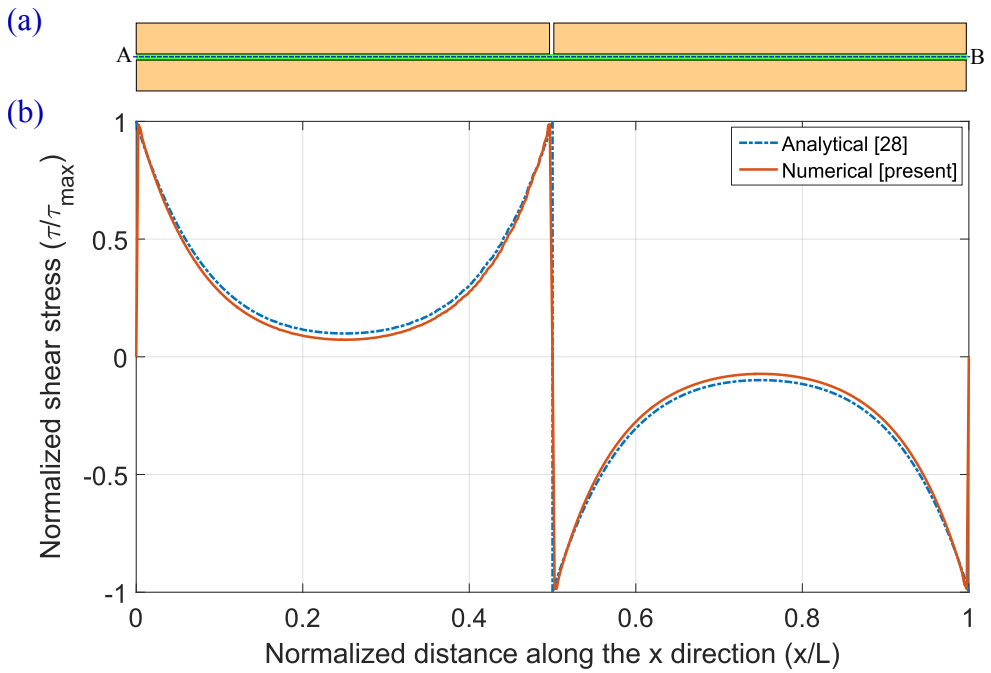

Figure 3: Shear stress distribution in polymer layer. (a) Schematic of the RVE highlighting path AB in the interphase along which the stress distribution is extracted. (b) Distribution of interfacial shear stress extracted from the present numerical analysis, as compared to results from the analytical model presented in [28].

3. RVE with functionally graded interphase modulus

Functional grading of the Young's modulus of a material along the desired directions is usually performed to achieve the desired (uniform) stress distribution by ironing out the peak stresses. In order to eliminate the areas of stress concentration a soft material is required around those areas. The soft nature of the interphase can be achieved by reducing the elastic modulus. Simultaneously, the load carrying capacity is maintained by tailoring the elastic modulus in the rest of the region. In this study, the modulus of the interphase is engineered to reduce the peak interfacial stresses around the tablet edges. The objective is achieved, by continuously varying the elastic modulus of the polymer as shown in Fig. 4. The selected representative volume element is shown in Fig. 4(a), whereas, smooth variation of the elastic modulus in the interphase selected RVE is shown in Fig. 4(b).

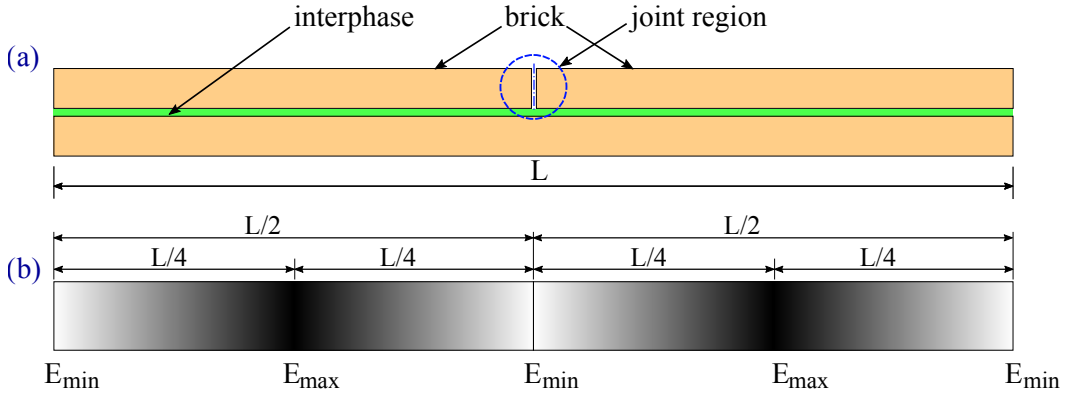

Figure 4: Schematic showing the variation of Young's modulus in the interphase of the RVE. (a) The selected representative volume element and (b) continuous variation of the elastic modulus in the interphase.

The modulus of the interphase is graded such that the elastic modulus at any point lies between the maximum (E_{max}) and minimum (E_{min}) values, see Fig. 4(b). Based on Fig. 3(b), regions of stress concentration are specified with lowest modulus E_{min}, see Fig. 4(b), such that peak stresses are reduced. On the other hand, highest modulus values (E_{max}) are specified in the regions of lowest stresses (see Fig. 3(b)), in order to incorporate the required stiffness to the composite structure. In this study, the elastic modulus of the interphase material is varied according to three different laws, namely: (i) linear, (ii) parabolic and (iii) bi-quadratic relations [30],

mentioned in Eqs. (1), (4) and (7), respectively.

Linear law

Let the Young's modulus of the interphase varies along the axial direction according to a linear law:

$$\mathrm{E}(x) = \mathrm{P}x + \mathrm{Q}. \tag{1}$$

where E(x) is the Young's modulus at a distance x from the vertical edge, see Fig. 4(b), L is the length of the tablet, and P and Q are the constants. Knowing the values of the Young's modulus at the vertical edges ($x = 0$ or $\frac{L}{2}$) and at the centre of the tablet ($x = \frac{L}{4}$), constants P and Q in the interval $0 \leq x \leq \frac{L}{4}$ are estimated as:

$$\mathrm{P} = \frac{(\mathrm{E_{max}} - \mathrm{E_{min}})}{(L/4)} \quad \text{and} \quad \mathrm{Q} = \mathrm{E_{min}}, \tag{2}$$

and when $\frac{L}{4} \leq x \leq \frac{L}{2}$:

$$\mathrm{P} = \frac{(\mathrm{E_{min}} - \mathrm{E_{max}})}{(L/4)} \quad \text{and} \quad \mathrm{Q} = 2\mathrm{E_{max}} - \mathrm{E_{min}}. \tag{3}$$

Parabolic law

Let the Young's modulus of the interphase varies along the axial direction according to a bi-quadratic law:

$$E(x) = \mathrm{R}x^2 + \mathrm{S}. \tag{4}$$

Constants R and S in the interval $0 \leq x \leq \frac{L}{4}$ are estimated as:

$$\mathrm{R} = \frac{(\mathrm{E_{max}} - \mathrm{E_{min}})}{(L/4)^2} \quad \text{and} \quad \mathrm{S} = \mathrm{E_{min}}. \tag{5}$$

and when $\frac{L}{4} \leq x \leq \frac{L}{2}$:

$$\mathrm{R} = \frac{(\mathrm{E_{min}} - \mathrm{E_{max}})}{(3L^2/16)} \quad \text{and} \quad \mathrm{S} = \frac{4\mathrm{E_{max}} - \mathrm{E_{min}}}{3}. \tag{6}$$

Bi-quadratic law

Let the Young's modulus of the interphase varies along the axial direction according to a parabolic law:

$$E(x) = \mathrm{T}x^4 + \mathrm{U}. \tag{7}$$

Constants T and U in the interval $0 \leq x \leq \frac{L}{4}$ are estimated as:

$$\mathrm{T} = \frac{(\mathrm{E_{max}} - \mathrm{E_{min}})}{(L/4)^4} \quad \text{and} \quad \mathrm{U} = \mathrm{E_{min}}. \tag{8}$$

and when $\frac{L}{4} \leq x \leq \frac{L}{2}$:

$$\mathrm{T} = \frac{(\mathrm{E_{min}} - \mathrm{E_{max}})}{(15L^4/256)} \quad \text{and} \quad \mathrm{U} = \frac{16\mathrm{E_{max}} - \mathrm{E_{min}}}{15}. \tag{9}$$

Variation of the elastic modulus in the rest of the interphase region can be estimated as a mirror image of the variation in $0 \leq x \leq \frac{L}{4}$. Such a variation of the elastic modulus along the length of interphase is plotted in Fig. 5(a), where a symmetry about the vertical axis in the first half of the interphase region can be observed and the pattern repeats in the second half.

The minimum and maximum values of the elastic modulus in a graded interphase are chosen as 0.5E and 1.5E, where E is the reference modulus listed in Table 1. The maximum and minimum elastic modulus locations are mentioned in Fig. 4(b). Distribution of the normalised interfacial shear stress along the axial direction according to various grading laws are plotted in Fig. 5(b). A close up of the peak interfacial shear stresses is also shown in the upper right corner of Fig. 5(b). According to Fig. 5(b), the peak stresses are significantly reduced by grading the interphase modulus. A maximum of 37% reduction in peak interfacial shear stress is estimated when the modulus is graded according to the linear law and a minimum of 20% reduction is observed with bi-quadratic grading. Furthermore, as shown in Fig. 5(b), the minimum shear stress in the interphase is found to be the highest with linear grading. This means that the gap between the maximum and minimum interfacial stress is reduced by ≈40%, which results in smooth distribution of

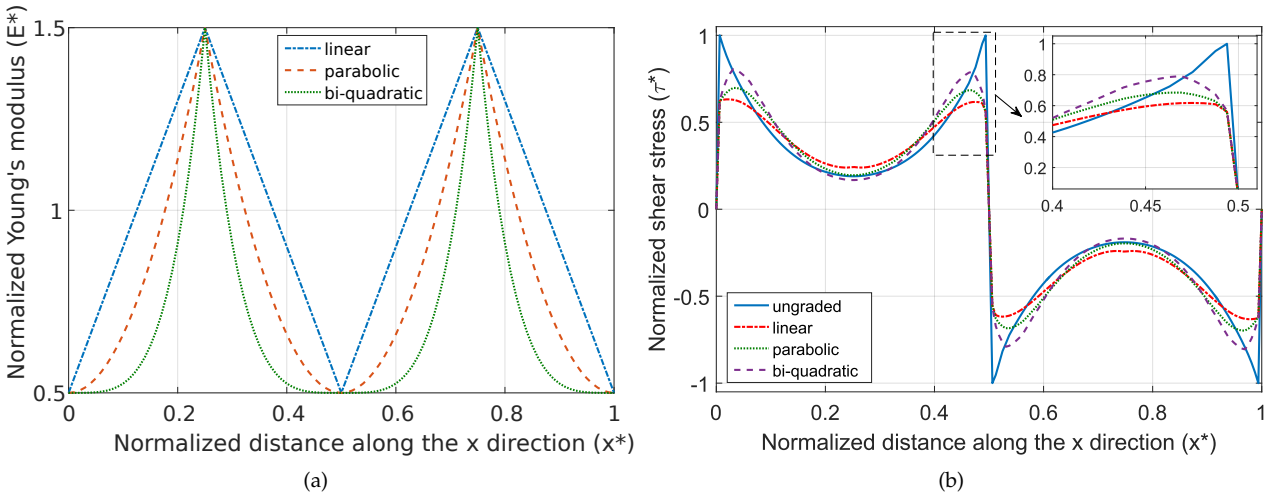

Figure 5: (a) Distribution of the elastic modulus along the length of the tablet considering linear parabolic and bi-quadratic grading laws. (d) Variation of normalised interfacial shear stress considering ungraded and graded interphases. The above three mentioned grading laws are tested to estimate the shear stress distribution.

interfacial shear stress as compared to the other cases. The elastic modulus of bi-quadratic graded interphase is observed to vary steeply around the regions of maximum modulus, i.e. $x = \frac{L}{4}$, and $\frac{3L}{4}$. Therefore, average stiffness of the bi-quadratic graded interphase is higher compared to the average stiffness of the linear graded interphase. As a result, stress transfer is more efficient and hence the stress peaks are much lower with linear graded interphase. Hence, nacre structure with linearly graded interphase yields lowest peak stress and hence the interphase absorbs much higher energy before the failure and tablet pull out. To summarise, the fracture toughness of the nacre structure with engineered interphase is much higher compared to interphase layer with homogeneous elastic modulus.

4. Parametric studies

In order to design efficient nacre mimicked structures, it is crucial to understand the influence of various parameters on the interfacial shear stress distribution. Therefore, a parametric study is conducted here to investigate the influence of: (i) overlap length, (ii) interphase modulus and (iii) interphase thickness and their combination, on the interfacial stress distribution of nacre structure.

4.1. Influence of overlap length

Overlap length in the brick-mortar structure is related to the positioning of adjacent bricks. A 100% overlap indicates placing one brick over another, such that there is no offset between their vertical edges. While a 50% overlap refers to an offset which is equal to half of the brick length and a 10% overlap indicates that the length of overlap region for the bricks is distributed as 0.9L and 0.1L. The overlap length plays an important role in the load transfer between the bricks. Therefore, the overlap length is varied from 50% to 10% of the tablet length. Distribution of the interfacial shear stress with different overlap lengths is plotted in Fig. 6(a). All other parameters including the mechanical properties and the dimensions of the RVE kept constant while varying the overlap length.

When the overlap length is 50% of the tablet length, the interfacial stress distribution is symmetric about a vertical axis at the centre of RVE. However, as the overlap length is gradually varied, the symmetry of stress distribution is lost, as shown in Fig. 6(a). The peak of the interfacial shear stress shifts towards the region with smaller overlap. This is expected, because for the constant external displacement load, the available stress transfer area for the brick with small overlap length decreases with decrease in overlap length. As a result, the peak interfacial stress gradually increases with decrease in overlap length. For instance, the peak shear stress increases by 3%, 8% and 27%, when the overlap length on one of the tablets is reduced to 40%, 30% and 20%, respectively. Variation of the peak stresses with %overlap length is plotted in Fig. 6(b). Based on Fig. 6(b), the peak stresses are observed to be exponentially increasing when the overlap length is less than 30%, and almost increased by 100% when the overlap reduces to 10%. To summarise, when overlap length increases, peak interfacial stresses reduces and reaches a minimum around 50% overlap length. This is because the load distribution will be more uniform when the core and overlap region are equal. In the natural nacre structure, found in the shell of red abalone, the average overlap is around 33% [6]. According to the present study, when the %overlap is more than 30, the reduction in peak interfacial stress is less than 8%, which is not significant. Therefore, the present study recommends a minimum overlap of 30% for efficient load transfer.

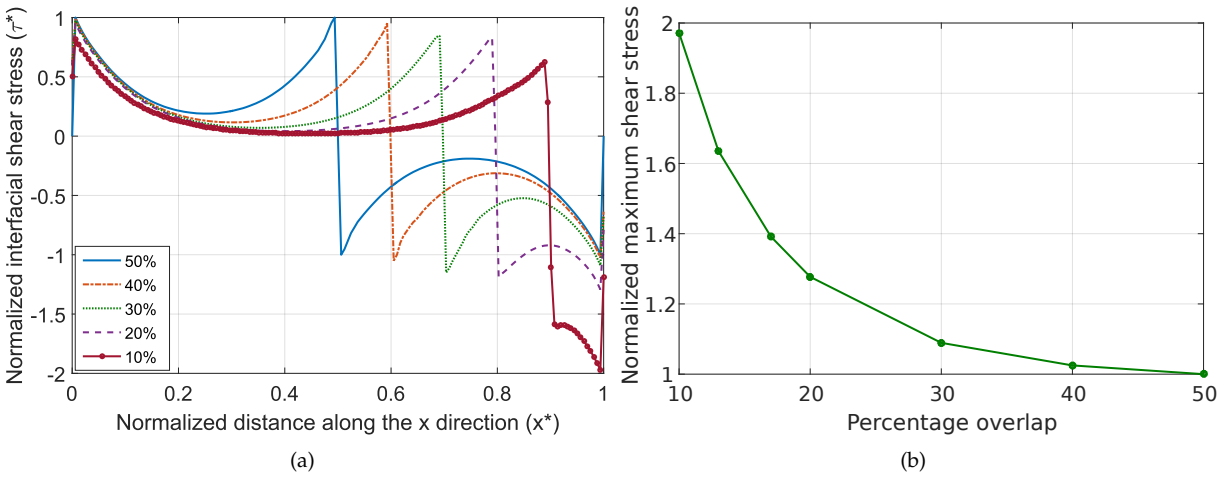

Figure 6: (a) Distribution of normalised interfacial stress for different overlap lengths. (b) Variation of the normalised peak interfacial shear stress with percentage overlap length.

4.2. *Influence of interphase modulus*

In order to investigate the influence of the elastic modulus on the interfacial shear stress distribution, the polymer modulus is varied from 0.2E to 10E, where E is of the reference modulus, while maintaining an overlap of 50% and retaining all the other parameters mentioned in Table 1. Distribution of the interfacial shear stress for various values of interphase modulus is shown in Fig. 7(a). The variation in Fig. 7(a) is observed to be symmetric as an overlap of 50% is considered in all the cases. Variation of the peak interfacial shear stress with elastic modulus is plotted in Fig. 7(b), where a close up is also shown. When the elastic modulus of the interphase layer is less than the reference modulus, peak stresses are observed to be reduced near the edges of the tablets and the stresses became smoother over the tablet length. The peak shear stresses are estimated to be reduced by 70% when the elastic modulus is reduced by 50% of its reference value, see the close up in Fig. 7(b). Furthermore, the reduction in peak interfacial stresses are found to be 50% and 30%, when the modulus is reduced to 70% and 80% of its reference value, respectively.

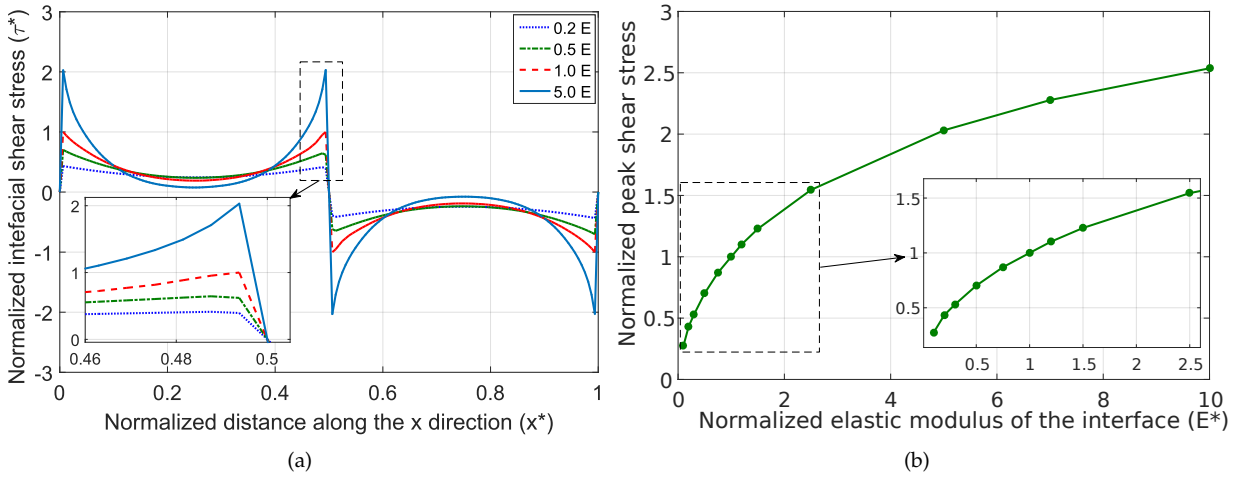

Figure 7: (a) Distribution of normalised interfacial stress with different elastic moduli. (b) Variation of the normalised peak interfacial shear stress with normalised elastic modulus of the interphase.

Alternately, with increase in elastic modulus, the peak interfacial stresses are found to increase exponentially, and they are concentrated around the edges of the tablets. This is because, the increase in interphase modulus leads to stiffening of the interphase layer and hence the load transfer is not smooth. Major load is absorbed in the regions around the edges of the tablets, resulting in stress concentration in those areas. The increase in peak interfacial stress is estimated to be 10% and 22%, when the modulus is increased by 20% (1.2E) and 50% (1.5E), respectively, which is not significant, as compared to 50% reduction in peak stresses with 50% reduction in the elastic modulus (0.5E). With further increase in elastic modulus the peak interfacial stress continue increase. For instance, when the modulus of the interphase is increased to 2.5E (150% rise), the peak

stress is found to be 55% more than its reference value, while when the modulus is raised to 5E (400% rise), the peak interfacial stresses are estimated to be increased by 100%. However, the rise is observed to be flat beyond 500% rise in elastic modulus, as 900% increase in modulus (10E) results in only 150% increase in peak stress.

The above study indicates that the peak interfacial stress in the interphase layer of brick-mortar structure is more responsive to reduction in interphase modulus, compared to its rise. This is a required property of the nacre structure, since lower modulus values reduce the stress peaks and homogenise the interfacial stresses. Furthermore, a lower interphase modulus helps in the participation of larger area of interphase in shear transfer, which leads to more uniform load distribution and hence large deformations before failure, enhancing the fracture toughness. On the other hand, the load carrying capacity and hence the strength of the brick-mortar structure reduces with decrease in elastic modulus. The decrease in strength can be compensated by providing the hardening mechanisms mentioned in the introduction Section 1. The hardening mechanisms makes the material strong after some initial deformation. Such hardening mechanisms exists in the natural nacre. Furthermore, a higher elastic modulus is not desirable, because it leads to creation of areas of stress concentration and higher peak stresses. In addition, the composite structure becomes more stiffer with higher elastic modulus values, and hence the load transfer between the tablets is not efficient, which could lead to the breakage of tablets close to the areas of traction boundary, before any significant deformation. Based on the above analysis, a soft interphase layer with hardening mechanisms is desirable to enhance unique load transfer mechanism of brick-mortar structure. Lower elastic modulus of the interphase leads to a tough structure and higher modulus makes it strong. Hence, the interphase modulus is required to be carefully engineered; for instance, functional grading discussed in Section 3, to arrive at an unique and efficient load transfer mechanism with significantly enhanced strength and toughness of nacreous material.

4.3. Influence of interphase thickness

In order to investigate the influence of interphase thickness, various thicknesses of interphase layer between 0.2t-10t are considered, where t is the reference thickness mentioned in Table 1, and rest of the parameters remains same.

Variation of the interfacial shear stress for various thicknesses is plotted in Fig. 8(a). As depicted in Fig. 8(a), the peak interfacial stress sharply rises with decrease in interphase thickness. Figure 8(b) shows a distribution of the peak interfacial stresses with thickness. A 50% decrease in thickness (0.5t) resulted in a 40% increase in the peak shear stress, and an 80% reduction (0.2t) yielded 150% increase, see the close up in Fig. 8(b). Hence, the composite structure is observed to be sensitive to reduction in interphase thickness. On the other hand, with an increase in interphase thickness, the interfacial stress distribution is observed to be more homogeneous, where the peak shear stresses are noticed to drop drastically. When the polymer layer thickness is increased by 50% (1.5t), the peak shear stress is decreased by 20% and for 100% increase in thickness (2t), the peak stresses are observed to be drop by 33%. The trend is observed to continue, where with an increase of 900% (10t), the peak shear stress became one-fourth of the initial value. This behaviour is expected, because with increase in thickness of the interphase, more area is available to transfer the same load and vice-versa. Hence, the peak shear stresses reduces by increasing the interphase thickness.

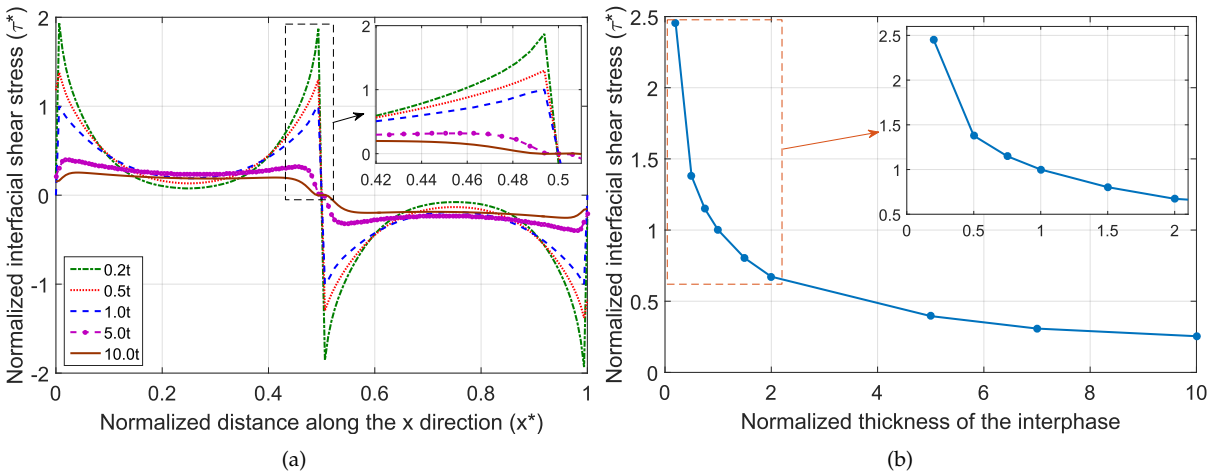

Figure 8: (a) Distribution of normalised interfacial stress with different interphase thicknesses. (b) Variation of the normalised peak interfacial shear stress with normalised thickness of the interphase.

4.4. *Influence of combined parameters*

After understanding the influence of overlap length, elastic modulus and interphase thickness individually on the stress transfer characteristics of brick-mortar structure, knowledge on the influence of a combination these parameters on the mechanical behaviour will be useful to come up with efficient designs.

In order to study the effect of combined thickness and elastic modulus of the interphase, on the interfacial shear stress distribution, interphase thickness is varied from 0.5t to 2t, where t is the reference thickness. For a given interphase thickness, elastic modulus is varied between 0.1E to 1.5E, where E is the reference modulus. The distribution of interfacial shear stress at 0.5t and 2t for different values of elastic modulus are presented in Figs. 9(a) and (b), respectively. According to Fig. 9, for given thickness, a uniform interfacial stress with

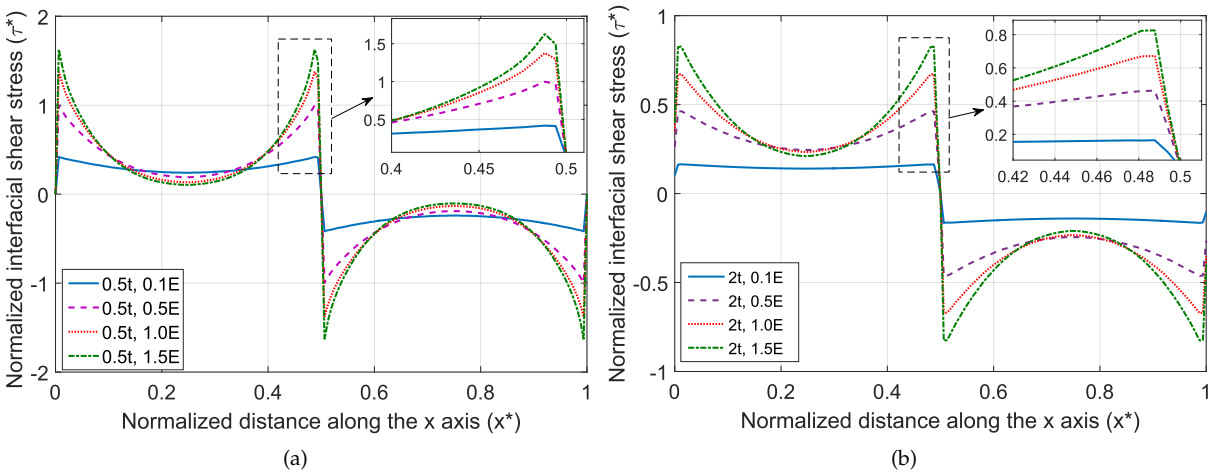

Figure 9: Distribution of normalised interfacial shear stress along the axial direction for different elastic moduli, considering interphase thickness equal to (a) 0.5t and (b) 2t.

reduced peak stresses can be achieved by reducing the elastic modulus values. On the other hand, increasing the elastic modulus is observed to have a reverse effect on the stress distribution, see Section 4.2. Based on Fig. 9(a), considering an interphase thickness of 0.5t, the peak interfacial stress estimated to be ≈1.5 times to that of the reference peak stress, i.e the peak stress value corresponding to 1.0E. However, the above peak stress was reduced to the reference value by decreasing the elastic modulus to 0.5E, see the close up in 9(a). Therefore, the peaks of the interfacial stresses can be suitably tailored by selecting the appropriate thickness and elastic modulus combination to arrive at the desirable performance characteristics of brick-mortar structure. The distribution of normalised interfacial shear stress for different values of elastic modulus, considering 2t are shown in Fig. 9(b).

The effect of combined overlap length and elastic modulus on the interfacial shear stress distribution is shown in Fig. 10. Plots in Fig. 10 are generated by varying the elastic modulus for a given overlap length. Several overlap lengths are considered, however, plots for 20% and 40% overlap, by varying the elastic modulus in the range 0.1E to 1.5E are shown in Fig. 10(a) and (b), respectively. The interfacial shear stress distribution for a specified overlap length can be smoothened by suitably reducing the elastic modulus. The peak stresses are observed to small in the larger overlap region, while they are high near the short overlap region. Such large stress peaks in the small overlap region can be bring down by reducing the elastic modulus accordingly.

The combined effect of interfacial thickness overlap length is shown in Fig. 11, by varying the interphase thickness between 0.5t to 1.5t, for a given overlap length.Several overlap lengths are studied, however plots with 40% and 20% overlap for different values of interphase thickness are plotted in Figs. 11(a) and (b), respectively. For all overlap lengths, the peak interfacial stresses reduces by increasing the interphase thickness. Furthermore, thickness values more than 't' smothens the shear stress distribution by reducing the stress peaks. Therefore, for a given overlap length the interphase thickness can be suitably tailored to achieve the desired interfacial shear stress distribution.

To summarise, the parametric study helps to tune and select the required parameters for the expected interfacial shear shear stress distribution, while designing the nacreous structures.

5. Applications

Nacre-like brick-mortar analogy has been successfully extended to arrive at a variety of composites structures, like: graphene based artificial nacre [31, 32], layered structures [33], fibre and sheet-like structures [25], composites for bio-medical applications [34, 35, 36], to name a few. An overview of nacre-inspired composites with

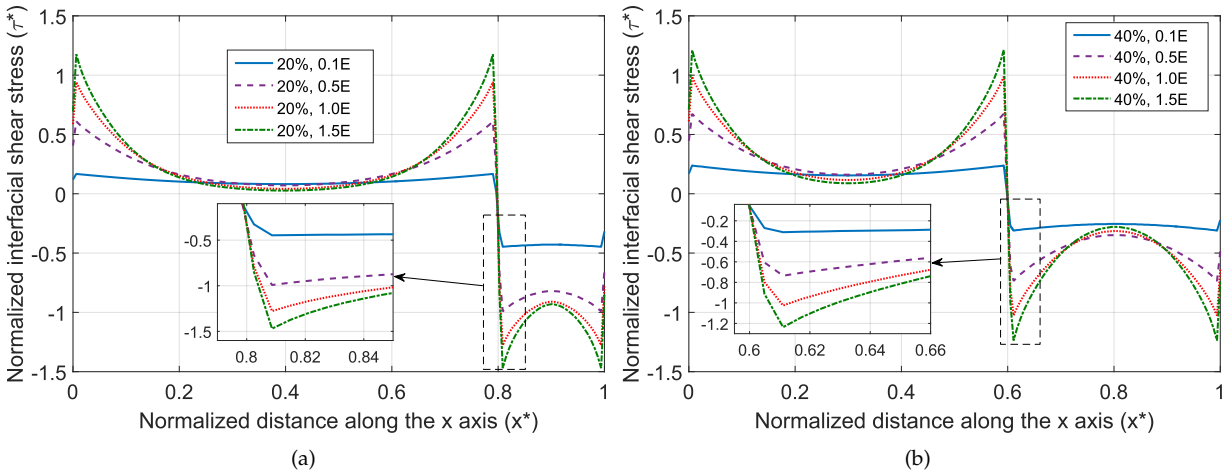

Figure 10: Distribution of normalised interfacial shear stress along the axial direction for different elastic moduli, considering an overlap of (a) 20% and (b) 40%.

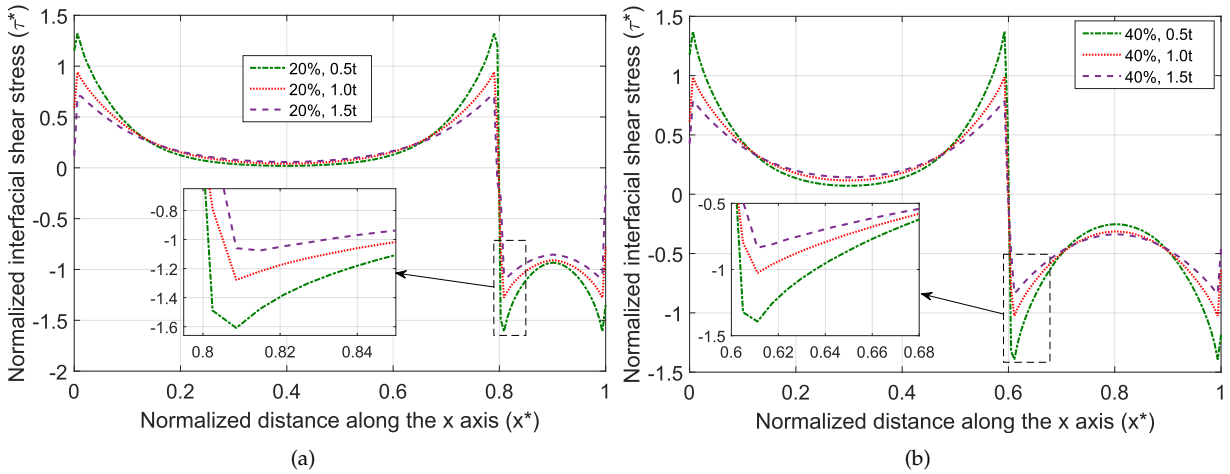

Figure 11: Distribution of normalised interfacial shear stress along the axial direction for different interphase thicknesses, considering an overlap of (a) 20% and (b) 40%.

better mechanical performance is available at [37, 38]. However, nacreous structure as a bulk material is yet to be reported. Therefore, we made an attempt here to design a nacreous structure based on the material combination used in metal matrix composites (MMC). The main reason behind selection of MMC is its similarity with two-material system as in nacre, i.e., reinforcement and matrix. In MMC the reinforcement is a strong and brittle material, while the matrix is relatively soft and ductile in nature.

In this study, Aluminium Silicon-carbide (AlSiC) and Magnesium Silicon-carbide, popular metal matrix composites are selected for the analysis. The bricks are made up of Silicon-carbide, whereas, the matrix material is chosen as either Aluminium or Magnesium. Silicon carbide (SiC) manufactured by tape casting or slip-casting methods [39, 40]. The adopted volume fraction in the practical AlSiC-9 composite structure is 63:37 [40]. Whereas, the ratio of aragonite brick and polymer in the nacre structure is 95:5. Therefore, simulations are performed for both volume fractions and the results are compared. However, the interphase thickness in traditional layered materials is of the order of centimetres to millimetres, which is 3-5 orders of magnitude thicker, compared to that of the thickness of interphase in nacre structure (micro-meters).

Constituent	Young's modulus (GPa)	Poisson's ratio	Permissible shear stress (MPa)
Silicon carbide (brick)	410	0.14	—
Magnesium (mortar/matrix)	45	0.35	140
Aluminium (mortar/matrix)	71	0.33	207

Table 2: Material properties.

The numerical analysis is performed in the similar lines discussed in Section 2. Material properties of Silicon carbide, Magnesium and Aluminium used in the numerical analysis are listed in Table 2. Distribution of the interfacial shear stress along the length of the tablet are plotted in Fig. 12, which indicates a similar trend as nacre structure. Based on Fig. 12(a), the shear stresses are observed to be concentrated near the tablet edges when the brick and mortar volume fraction is 95:5. However, with the brick and mortar volume fraction of 66:34, the shear stress variation in Fig. 12(b), is more distributed as compared to the distribution in Fig. 12(a). Furthermore, the peak stresses with volume fraction 66:34 are observed to be lower as compared to peak stresses with volume fraction 95:5, see Fig. 12(c).

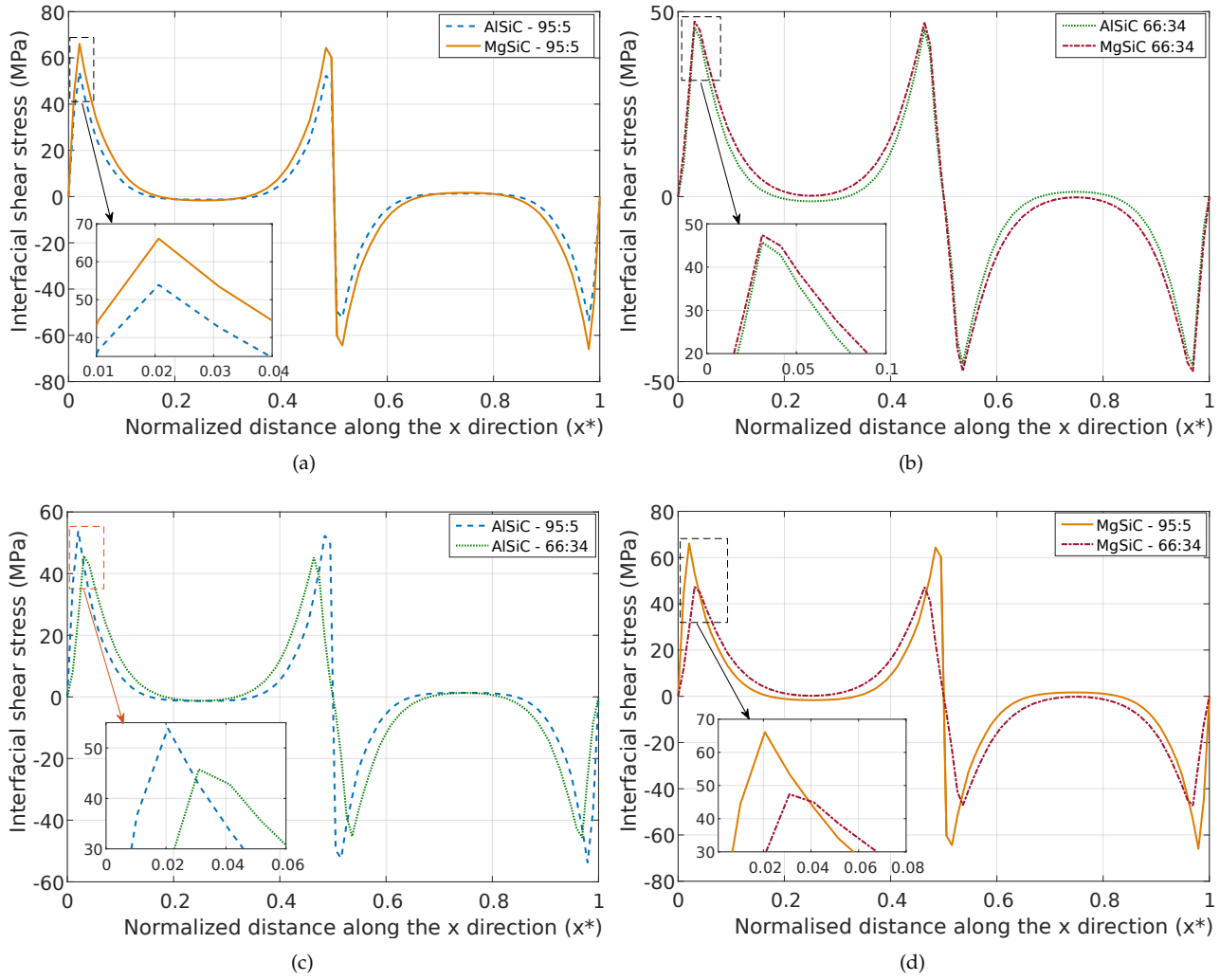

Figure 12: Shear stress distribution in polymer layer for percentage overlap and polymer modulus variation.

The shear stress limit in nacre matrix is 50 MPa that is shown by point in all the schematics. For aluminium and magnesium, the maximum shear stress limits are 140 MPa and 207 MPa respectively hence nacreous composite having Al and Mg as matrix material can sustain much higher load than the natural nacre. This study shows that the material combination used in metal matrix composites can be applied in brick and mortar structure. With this approach, the nacreous structure could be used as bulk material. This Composite can also be applied to the structural application.

6. Conclusions

In summary, the shear stress distribution in the polymer layer distribution is established using numerical method. The shear stress distribution in the polymer matrix is homogenised by grading the modulus of the polymer while maintaining the stiffness of the composite. The grading of polymer modulus can help distributive the load in the polymer layer homogenously, eliminating the areas of stress concentration. The parametric study revealed the effect of polymer layer thickness, polymer modulus and percentage overlap on the non-homogeneous stress distribution. The parametric study could serve as a design guideline for designing nacreous composite for parameter selection. The parametric study also shows that the parameters can

be mutually adjusted to maintain the stress homogeneity and stiffness of the composite. Furthermore, to use nacre as a bulk material, material combination for the bricks and matrix is suggested that showed promising results. The study and analysis of biological material are promising and it has inspired many people to mimic these structures but they are not able to match the performance of natural material. Yet the study of theses material has made it clear that by multiscale structure material made up of weak constituents can deliver excellent mechanical performance.

Very accurate data is now available about the microstructure of nacre and its mechanical properties through the advancement of experiments. But there are still aspects of the structure which require further research like the specific role of mineral bridges, Nano asperities and nanograins in enhancing the mechanical properties. Furthermore, general constitutive laws regarding various loading are not yet available. With the joint application of experiments, simulations and analytical approach, the above-mentioned problems might be solved to some extent. Fracture behaviours of nacre can be studied which might help to improve its fracture characteristics. The structure of nacre is developed and optimized over a million years of evolution. To active the level of sophistication and performance on nacre on artificial materials is still to be seen.

Acknowledgements

PRB is thankful.

References

[1] Reza Rabiei, Sacheen Bekah, and Francois Barthelat. Failure mode transition in nacre and bone-like materials. *Acta biomaterialia*, 6(10):4081–4089, 2010.

[2] Ahmad Khayer Dastjerdi, Reza Rabiei, and Francois Barthelat. The weak interfaces within tough natural composites: experiments on three types of nacre. *Journal of the mechanical behavior of biomedical materials*, 19:50–60, 2013.

[3] Tilman E Schäffer, Cristian Ionescu-Zanetti, Roger Proksch, Monika Fritz, Deron A Walters, Nils Almqvist, Charlotte M Zaremba, Angela M Belcher, Bettye L Smith, Galen D Stucky, et al. Does abalone nacre form by heteroepitaxial nucleation or by growth through mineral bridges? *Chemistry of Materials*, 9(8):1731–1740, 1997.

[4] Albert Yu-Min Lin, Po-Yu Chen, and Marc André Meyers. The growth of nacre in the abalone shell. *Acta Biomaterialia*, 4(1):131–138, 2008.

[5] Fabian Heinemann, Malte Launspach, Katharina Gries, and Monika Fritz. Gastropod nacre: structure, properties and growthâ€"biological, chemical and physical basics. *Biophysical chemistry*, 153(2-3):126–153, 2011.

[6] F Barthelat and HD Espinosa. An experimental investigation of deformation and fracture of nacre–mother of pearl. *Experimental mechanics*, 47(3):311–324, 2007.

[7] S Xiao, SA. Edwards, and F. Gräter. A new transferable forcefield for simulating the mechanics of caco3 crystals. *The Journal of Physical Chemistry C*, 115(41):20067–20075, 2011.

[8] N Zhang, S Yang, L Xiong, Y Hong, and Y. Chen. Nanoscale toughening mechanism of nacre tablet. *Journal of the Mechanical Behavior of Biomedical Materials*, 53:200–209, 2016.

[9] Mehmet Sarikaya and Ilhan A Aksay. Biomimetics. design and processing of materials. Technical report, WASHINGTON UNIV SEATTLE DEPT OF MATERIALS SCIENCE AND ENGINEERING, 1995.

[10] AP Jackson, Julian FV Vincent, and RM Turner. The mechanical design of nacre. *Proceedings of the Royal society of London. Series B. Biological sciences*, 234(1277):415–440, 1988.

[11] F Barthelat, H Tang, PD Zavattieri, CM Li, and HD. Espinosa. On the mechanics of mother-of-pearl: A key feature in the material hierarchical structure. *Journal of the Mechanics and Physics of Solids*, 55(2):306–337, 2007.

[12] François Barthelat, Chun-Ming Li, Claudia Comi, and Horacio D Espinosa. Mechanical properties of nacre constituents and their impact on mechanical performance. *Journal of Materials Research*, 21(8):1977–1986, 2006.

[13] John Donald Currey. Mechanical properties of mother of pearl in tension. *Proceedings of the Royal society of London. Series B. Biological sciences*, 196(1125):443–463, 1977.

[14] Ko Okumura and P-G De Gennes. Why is nacre strong? elastic theory and fracture mechanics for biocomposites with stratified structures. *The European Physical Journal E*, 4(1):121–127, 2001.

[15] RZ Wang, Z Suo, AG Evans, N Yao, and IA Aksay. Deformation mechanisms in nacre. *Journal of Materials Research*, 16(9):2485–2493, 2001.

[16] Huajian Gao, Baohua Ji, Ingomar L Jäger, Eduard Arzt, and Peter Fratzl. Materials become insensitive to flaws at nanoscale: lessons from nature. *Proceedings of the national Academy of Sciences*, 100(10):5597–5600, 2003.

[17] F Song and YL Bai. Effects of nanostructures on the fracture strength of the interfaces in nacre. *Journal of Materials Research*, 18(8):1741–1744, 2003.

[18] AG Evans, Z Suo, RZ Wang, IA Aksay, MY He, and JW Hutchinson. Model for the robust mechanical behavior of nacre. *Journal of Materials Research*, 16(9):2475–2484, 2001.

[19] Dinesh R Katti, Shashindra Man Pradhan, and Kalpana S Katti. Modeling the organic-inorganic interfacial nanoasperities in a model bio-nanocomposite, nacre. *Reviews on Advanced Materials Science*, 6(2):162–168, 2004.

[20] R Menig, MH Meyers, MA Meyers, and KS Vecchio. Quasi-static and dynamic mechanical response of haliotis rufescens (abalone) shells. *Acta Materialia*, 48(9):2383–2398, 2000.

[21] Zuoqi Zhang, Yong-Wei Zhang, and Huajian Gao. On optimal hierarchy of load-bearing biological materials. *Proceedings of the Royal Society B: Biological Sciences*, 278(1705):519–525, 2010.

[22] Xiaodong Li, Wei-Che Chang, Yuh J Chao, Rizhi Wang, and Ming Chang. Nanoscale structural and mechanical characterization of a natural nanocomposite material: the shell of red abalone. *Nano letters*, 4(4):613–617, 2004.

[23] George Mayer. Rigid biological systems as models for synthetic composites. *Science*, 310(5751):1144–1147, 2005.

[24] Hong-Bin Yao, Zhi-Hua Tan, Hai-Yu Fang, and Shu-Hong Yu. Artificial nacre-like bionanocomposite films from the self-assembly of chitosan–montmorillonite hybrid building blocks. *Angewandte Chemie International Edition*, 49(52):10127–10131, 2010.

[25] SP Kotha, Y Li, and N Guzelsu. Micromechanical model of nacre tested in tension. *Journal of materials science*, 36(8), 2001.

[26] Dinesh R Katti and Kalpana S Katti. Modeling microarchitecture and mechanical behavior of nacre using 3d finite element techniques part i elastic properties. *Journal of Materials Science*, 36(6):1411–1417, 2001.

[27] Horacio D Espinosa, Jee E Rim, Francois Barthelat, and Markus J Buehler. Merger of structure and material in nacre and bone–perspectives on de novo biomimetic materials. *Progress in Materials Science*, 54(8):1059–1100, 2009.
[28] Yong Ni, Zhaoqiang Song, Hongyuan Jiang, Shu-Hong Yu, and Linghui He. Optimization design of strong and tough nacreous nanocomposites through tuning characteristic lengths. *Journal of the Mechanics and Physics of Solids*, 81:41–57, 2015.
[29] JA. Nairn. On the use of shear-lag methods for analysis of stress transfer in unidirectional composites. *Mechanics of Materials*, 26:63–80, 1997.
[30] N Stein, J Felger, and W Becker. Analytical models for functionally graded adhesive single lap joints: A comparative study. *International journal of adhesion and adhesives*, 76:70–82, 2017.
[31] Yuanyuan Zhang, Shanshan Gong, Qi Zhang, Peng Ming, Sijie Wan, Jingsong Peng, Lei Jiang, and Qunfeng Cheng. Graphene-based artificial nacre nanocomposites. *Chemical Society Reviews*, 45(9):2378–2395, 2016.
[32] Yang Wang, Hao Yuan, Piming Ma, Huiyu Bai, Mingqing Chen, Weifu Dong, Yi Xie, and Yogesh S Deshmukh. Superior performance of artificial nacre based on graphene oxide nanosheets. *ACS applied materials & interfaces*, 9(4):4215–4222, 2017.
[33] Paul Podsiadlo, Stephen Paternel, Jean-Marie Rouillard, Zhengfei Zhang, Jaebeom Lee, Jung-Woo Lee, Erdogan Gulari, and Nicholas A Kotov. Layer-by-layer assembly of nacre-like nanostructured composites with antimicrobial properties. *Langmuir*, 21(25):11915–11921, 2005.
[34] Ethan Michael Gerhard, Wei Wang, Caiyan Li, Jinshan Guo, Ibrahim Tarik Ozbolat, Kevin Michael Rahn, April Dawn Armstrong, Jingfen Xia, Guoying Qian, and Jian Yang. Design strategies and applications of nacre-based biomaterials. *Acta biomaterialia*, 54:21–34, 2017.
[35] Hiromichi Takebe, Sengo Kobayashi, Hiromichi Aono, and Saeki Yamamuro. Fabrication and characterization of natural/synthesized, micro-, and nanostructured materials for biomedical applications. In *Nanostructures for Novel Therapy*, pages 81–106. Elsevier, 2017.
[36] Sung Chan Yoo, Yoon Kyung Park, Changsik Park, Hojin Ryu, and Soon Hyung Hong. Biomimetic artificial nacre: Boron nitride nanosheets/gelatin nanocomposites for biomedical applications. *Advanced Functional Materials*, 28(51):1805948, 2018.
[37] Flavia Libonati et al. Bio-inspired composites: using nature to tackle composite limitations. *Advanced Engineering Materials and Modeling*, pages 165–190, 2016.
[38] Hewei Zhao, Zhao Yang, and Lin Guo. Nacre-inspired composites with different macroscopic dimensions: strategies for improved mechanical performance and applications. *NPG Asia Materials*, 10(4):1, 2018.
[39] Maximilien E Launey, Etienne Munch, Daan Hein Alsem, Eduardo Saiz, Antoni P Tomsia, and Robert O Ritchie. A novel biomimetic approach to the design of high-performance ceramic–metal composites. *Journal of the Royal Society Interface*, 7(46):741–753, 2009.
[40] Jianfeng Wang, Qunfeng Cheng, and Zhiyong Tang. Layered nanocomposites inspired by the structure and mechanical properties of nacre. *Chemical Society Reviews*, 41(3):1111–1129, 2012.